Effect of solvent on the magnetic properties of the high-temperature $V[TCNE]_x$ molecule-based magnet

Konstantin I. Pokhodnya,[1,2] Dusan Pejakovic,[2] Arthur J. Epstein,[2,3] and Joel S. Miller[1]
[1]*Department of Chemistry, University of Utah, 315 South 1400 East, Salt Lake City, Utah 84112-0850*
[2]*Department of Physics, The Ohio State University, 174 West 18th Street, Columbus, Ohio 43210-1106*
[3]*Department of Chemistry, The Ohio State University, 174 West 18th Street, Columbus, Ohio 43210-1106*
(Received 7 November 2000; published 2 April 2001)

The different magnetic behaviors of the $V[TCNE]_x$ (TCNE=tetracyanoethylene) magnet prepared via the reaction of TCNE and $V(CO)_6$ in CH_2Cl_2 and the solvent-free chemical vapor deposition (CVD) of TCNE and $V(CO)_6$ onto a glass substrate were determined. It was shown that the presence of noncoordinating CH_2Cl_2 solvent molecules in the structure of the $V[TCNE]_x$ magnet does not substantially influence the magnetic ordering temperature; however, it creates additional structural disorder. This results in a correlated spin-glass behavior in low magnetic fields ($H<100$ Oe) at helium temperatures, small remanence, and vanishing coercive fields at room temperature. In contrast, the CVD-prepared film has increased structural order. Quantitatively, the degree of disorder was analyzed in the framework of the random magnetic anisotropy model.

DOI: 10.1103/PhysRevB.63.174408 PACS number(s): 75.50.Xx, 75.50.Kj, 75.10.−b

I. INTRODUCTION

Advances in the science and technology of several classes of magnetic materials, including molecule-based magnets,[1] have occurred in the past decade. Today there are a few molecule-based magnets with magnetic ordering temperatures (T_c) above room temperature,[2] and these include $V[TCNE]_x$ (TCNE=tetracyanoethylene, $x\sim2$).[3,4] The $V[TCNE]_x$ magnet originally was synthesized via the reaction of TCNE and $V(C_6H_6)_2$ in CH_2Cl_2,[3] and later via the reaction of TCNE and $V(CO)_6$ in CH_2Cl_2.[4] This magnet forms instantaneously as an insoluble, amorphous powder containing approximately one half of a solvent molecule per V. Recently, $V[TCNE]_x$ has been deposited as a thin film on different substrates (including Si wafers) by a low-temperature chemical vapor deposition (CVD) method[5] that makes this material potentially applicable for producing devices via integrated microelectronic technology.

$V[TCNE]_x\cdot yS$ ($S=CH_2Cl_2$) has a spontaneous magnetization (M) at room temperature. The analysis of $M(T)$ using spin-wave theory suggested that the magnetic ordering temperature T_c is ~400 K; however, this is not achievable due to thermal decomposition of the sample at ~350 K.[6] Solvents that can coordinate with V [e.g., H_3CCN or C_4H_8O (tetrahydrofuran, THF)] introduce substantial structural and substitutional disorder that considerably suppresses T_c. This is attributed to blocking the superexchange pathways.[7] However, the role of noncoordinating solvents such as CH_2Cl_2 is unclear.

Herein, we report a comparative study of the $V[TCNE]_x$ magnet prepared via two alternative routes: the reaction of TCNE and $V(CO)_6$ in CH_2Cl_2 [bulk sample (**B**)], and solvent-free chemical vapor deposition of TCNE and $V(CO)_6$ resulting in the formation of the $V[TCNE]_x$ thin film on the surface of a glass substrate[3] [film sample (**F**)]. We show that the presence of noncoordinating CH_2Cl_2 solvent molecules in the structure of the $V[TCNE]_x$ magnet does not substantially influence T_c; however, it creates additional structural disorder that considerably modulates the magnetic properties at low temperatures.

II. EXPERIMENT

$V[TCNE]_x\cdot y(CH_2Cl_2)$ (**B**) (Ref. 3) and $V[TCNE]_x$ (**F**) (Ref. 5) were prepared according to the literature. The **F** film was deposited onto a glass substrate, removed from it by scraping with a nonmagnetic spatula, and both were used for magnetic measurements and thermoanalysis. All manipulations and reactions were performed in a Vacuum Atmospheres DriLab glove box (<1 ppm O_2 and <1 ppm H_2O). The CH_2Cl_2 used for the reaction was predried and distilled from the appropriate drying agents. Samples for magnetic measurements were loaded in airtight Delrin holders and packed with oven-dried quartz wool to prevent movement of each sample in its holder.

The 2–400 K dc magnetization and ac magnetic susceptibility were obtained using a Quantum Design MPMS-5XL 5 T superconducting quantum interference device (sensitivity=10^{-8} emu) magnetometer equipped with a reciprocating sample measurement system, low-field option, and continuous low-temperature control with enhanced thermometry features. The ac magnetic susceptibility was measured with a Lake Shore 7225 ac susceptometer in a 1 Oe ac field of (zero dc applied field) between 4–7900 Hz. Phase-sensitive lock-in detection allowed both the in-phase (χ') and out-of-phase (χ'') linear susceptibilities to be extracted.

To obtain reproducible results, especially at low magnetic fields, the magnetic history of the sample was completely erased. Since the paramagnetic state is not attainable due to sample decomposition, the sample was demagnetized at 300 K in an oscillating magnetic field with gradually decreasing amplitude down to 0.0 ± 0.1 Oe prior to each experiment. This procedure decreased the absolute value of residual magnetization down to ~0.1% of its saturation value and led to reproducible results in field-cooled (FC) and zero-field-cooled (ZFC) experiments. The dc magnetization was measured in various magnetic fields by cooling in zero field from

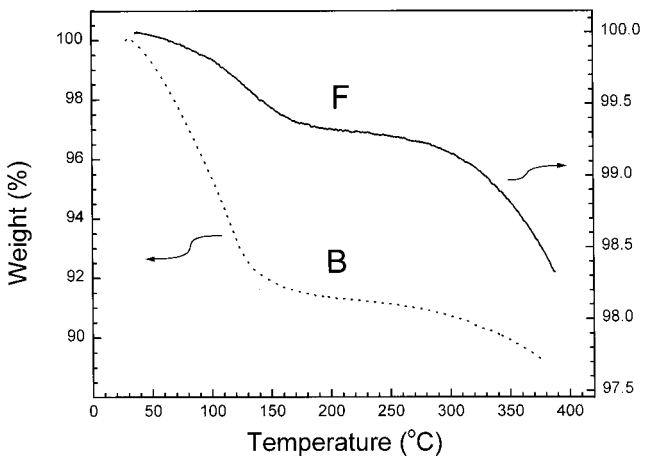

FIG. 1. TGA of $V[TCNE]_x \cdot y(CH_2Cl_2)$ (**B**) and $V[TCNE]_x$ film (**F**).

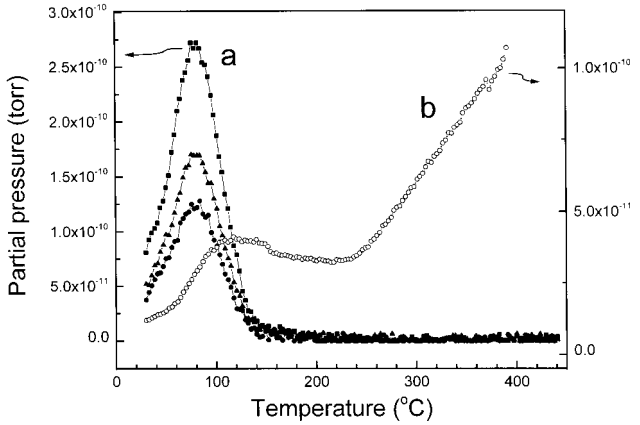

FIG. 2. Temperature dependence of the partial pressure of the ions in **B**: (a) originated from CH_2Cl_2, masses=83 (□); 84 (△); and 85 (●) and decomposition (b) from TCNE, mass=26(○).

320 K down to 2 K (ZFC), or by cooling in applied field from 300 to 2 K (FC). In both cases data were collected on warming.

The thermal properties were studied using a TA Instruments model 2050 thermogravimetric analyzer (TGA) equipped with a TA-MS Fison triple-filter quadrupole mass spectrometer to identify gaseous products with masses less than 300 amu. It is located in a DriLab glove box that uses argon to protect air-and moisture-sensitive samples. Samples were placed in an aluminum pan and heated at 20 °C/min under a continuous 10-mL/min nitrogen flow. High-resolution mass spectra were obtained using a Finnigan MAT 95 high-resolution mass spectrometer equipped with a Finnigan MAT ICIS II operating system.

III. EXPERIMENTAL RESULTS AND ANALYSIS

A. Thermal studies

The comparison of magnetic properties of $V[TCNE]_x$ films (**F**) with the solvent-containing bulk material (**B**) requires an accurate determination of solvent content. TGA analyses reveal that **B** samples begin to loose solvent immediately after heating above room temperature, Fig. 1(a). The maximum rate of solvent loss is achieved at 85–90 °C, and at 130 °C the weight loss almost ceases. At this temperature the partial pressure of the ions originating from the solvent molecule also vanishes (Fig. 2). Assuming $x=2$ and the sample has lost all solvent (~8.5%) the solvent content y for $V[TCNE]_2 \cdot y(CH_2Cl_2)$ is 0.34 ± 0.01, and its molecular mass is 336 g/mol.

It should be noted that at 75–80 °C the mass spectrometer begins registering ions with the mass of 26 amu (Fig. 2), corresponding to the loss of mass of CN^- that is attributed to $[TCNE]\cdot^-$ decomposition. The partial pressure CN^- reaches maximum at ~120 °C and then decreases gradually reaching the local minimum at ~225 °C. On further heating it starts to increase rapidly again, indicating that above 250 °C the decomposition process accelerates.

In contrast to the bulk sample **B**, the film **F**, due to the lack of solvent, has only very minor weight changes upon ramping up to 100 °C (<0.15%), attributed to instrument drift. Between 100–200 °C the film sample loses about 0.5% of its weight [Fig. 1(b)]. Cyanide (CN) or heavier ions that could be related to $[TCNE]\cdot^-$ decomposition, do not appear in the mass spectrum.[8] The only ion that is observed has a mass equal to 28 amu, and this is attributed to residual CO, a byproduct from the reaction between TCNE and $V(CO)_6$. High-resolution mass spectrometric data capable of distinguishing between CO (27.996 amu) and the N_2 (28.006 amu) purging gas confirmed that CO is present. Thus, CO is trapped in the $V[TCNE]_x$ polymeric network and released upon heating. Above 250 °C the thermal properties of the **F** film are similar to that of **B**. The weight loss accelerates and ions related to $[TCNE]\cdot^-$ decomposition appear in the mass spectrum.

Thus, TGA studies show that the solvent-containing $V[TCNE]_x$ (**B**) begins to decompose at a much lower temperature than the solvent-free film. Although CH_2Cl_2 is a noncoordinating solvent, it is probably trapped in the bulk and contributes to steric strain with respect to $[TCNE]^-$ coordination to V^{II}. Hence, some $[TCNE]\cdot^-$'s may not be bonded to V via all four CN groups. The CN groups that do not bond to V likely have weaker bonds and would be broken at lower temperatures, and the appearance of CN^- ions in the temperature range $75 < T < 200$ °C is a manifestation of this process. However, as the partial pressure of CN^- ions in this temperature interval is low ($\sim 10^{-11}$ Torr), the concentration of these defects is small.

B. Magnetic studies

The differences in structure and chemical composition of the **B** and **F** compounds impact the magnetic properties. **B** and **F** begin to decompose at ~350 K. Both **B** and **F** are ordered magnetically up to the decomposition temperature, which is estimated to be 400 K (vide infra). The decomposition results in irreversible structural and chemical composition changes that substantially suppress both T_c and the absolute value of magnetization upon thermal treatment.[3,5]

The temperature dependence of the magnetization in different applied fields for **B** reveals a pronounced field-

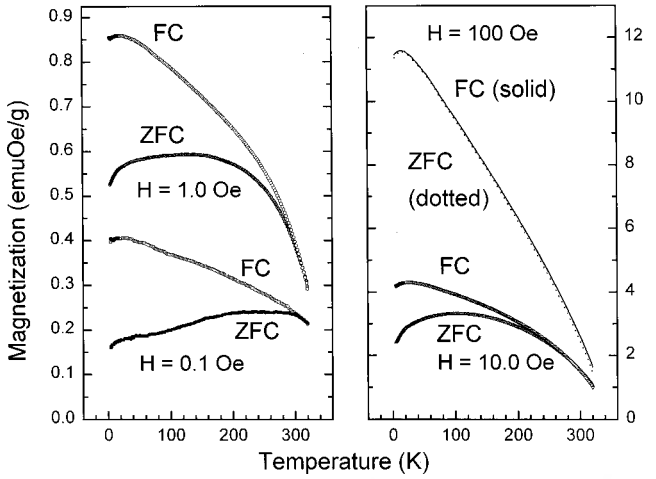

FIG. 3. Field-cooled (upper curves) and zero-field cooled (lower curves) magnetization of V[TCNE]$_x$ bulk samples as function of T at different magnetic fields.

dependent bifurcation of the FC and ZFC curves in $H < 100$ Oe, Fig. 3. The bifurcation temperature T_b decreases with increasing applied field and almost vanishes at 100 Oe. Below 100 Oe the ZFC $M(T)$ has a broad maximum that gradually shifts toward low temperatures with increasing H.

A distinct difference between ZFC and FC $M(T)$ in $H < 100$ Oe was also observed for **F** (Fig. 4). This difference, however, is only ~20% of that for **B**. In contrast to **B**, the shape of both the FC and ZFC $M(T)$ data as well as the position of bifurcation points are almost field independent for $H \leqslant 10$ Oe. Similar to **B**, the difference between FC and ZFC $M(T)$ data almost vanishes for $H > 100$ Oe. It should be noted that in all magnetic fields studied there is a sharp increase in ZFC magnetization at the $5 < H < 40$-K temperature interval, which is more pronounced in the **F** samples, and the absolute value of $M(T)$ is larger for the **B** samples with respect to the **F** samples.

The dependences of the in-phase (χ') and out-of-phase (χ'') components of the complex ac susceptibility measured

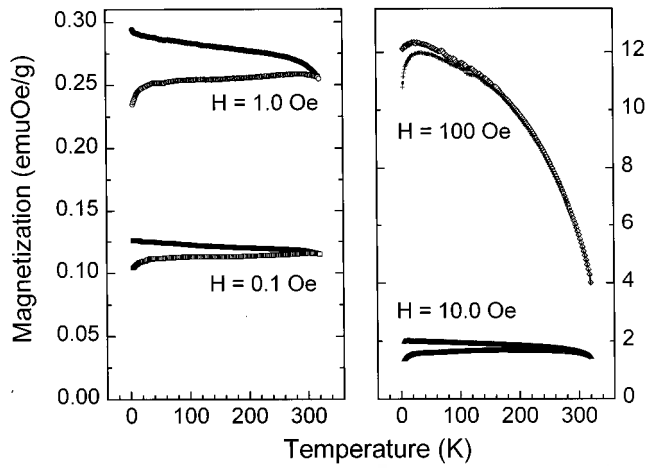

FIG. 4. Field-cooled (upper curves) and zero-field cooled (lower curves) magnetization of V[TCNE]$_x$**F** film sample as function of T at different magnetic fields.

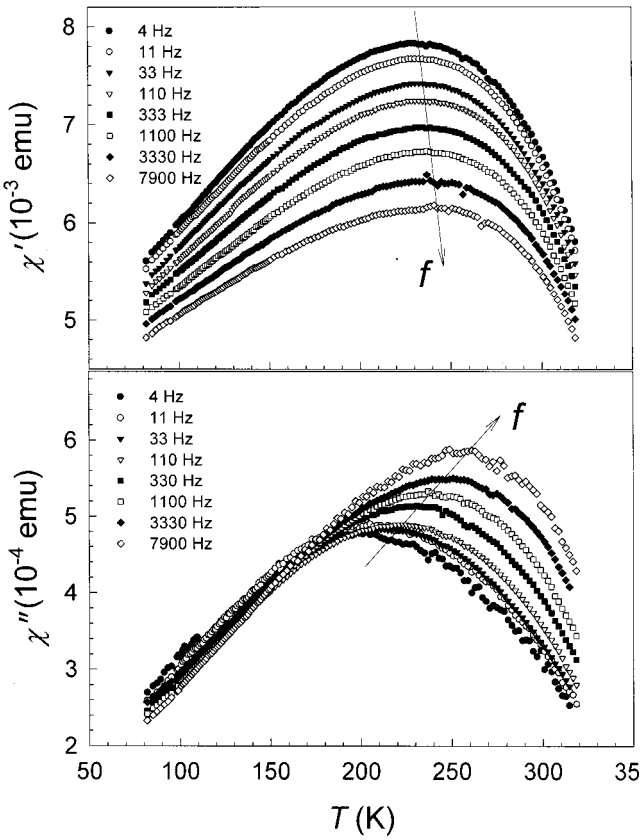

FIG. 5. Temperature dependence of V[TCNE]$_x \cdot 0.3(CH_2Cl_2)$ (**B**) χ' and χ'' in $H_{ac} = 1$ Oe at different frequencies (see legend).

at different frequencies (4–7900 Hz) for **B** are shown in Fig. 5. Both $\chi'(T)$ and $\chi''(T)$ display a broad peak at 250 and 200 K, respectively, resembling in shape the ZFC curve measured at 0.1 Oe (Fig. 3). Despite the difficulties in determining an accurate maximum in $\chi'(T)$ and $\chi''(T)$, a gradual shift toward higher temperatures can be clearly distinguished in the **B** samples as the measuring frequency increases. In contrast, **F** does not show similar frequency dependences on either component of ac-susceptibility (Fig. 6).

To establish a spontaneous moment, the remanent magnetization (M_r) was measured between 2–400 K. The sample was cooled in 500-Oe field (close to saturation) from 300–2 K, then the field was switched off, and $M_r(T)$ was measured while warming from 2–400 K [Fig. 7 (a)]. The $M_r(T)$ of **B** drops exponentially between 2–300 K. The $M_r(T)$ dependence can be fit to a sum of two exponential functions

$$M_r(T) = M_0 + A_1 \exp(-T/T_1) + A_2 \exp(-T/T_2)$$

with two characteristic temperatures $T_1 = 4.0$, $T_2 = 107$ K, and two preexponential factors $A_1 = 1.50$ and $A_2 = 2.37$ emu Oe/g. ($M_0 = 0.13$ emu Oe/g). Above 300 K, $M_r(T)$ begins dropping more sharply, revealing an irreversible structural magnetic transition with an onset at 360 K.

For $M_r(T)$ of **F** a sharp exponential drop also is observed in the much narrower temperature interval of 2–10 K [Fig. 7(b)], i.e., $M_r(T) \propto \exp[-T/T_3]$ with $T_3 \sim 2$ K. Above 10 K $M_r(T)$ decreases linearly to 300 K and then has a magnetic

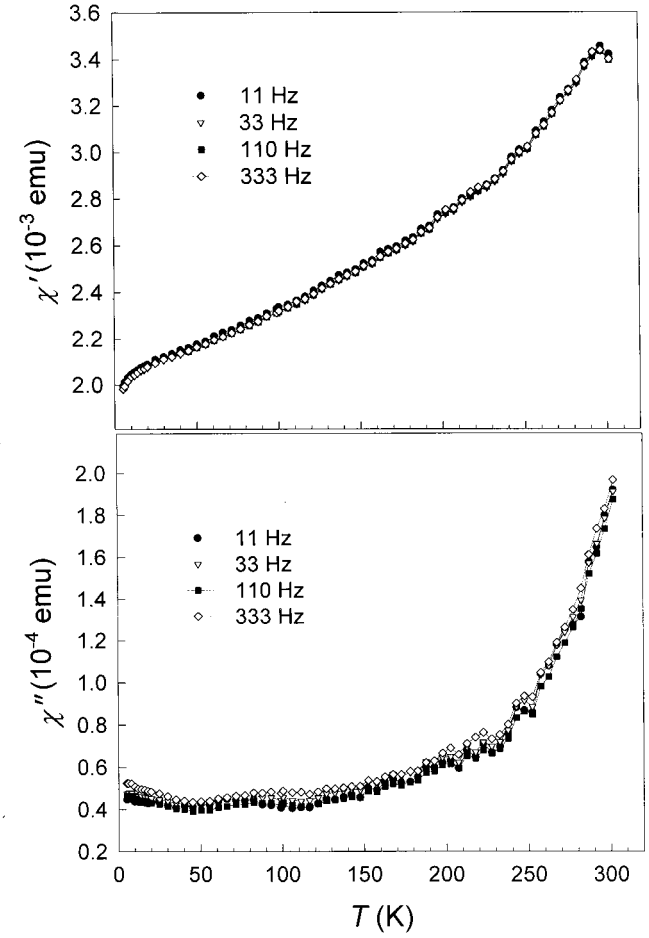

FIG. 6. $\chi'(T)$ and $\chi''(T)$ of the film sample (**F**) at 11, 33, 111, and 333 Hz.

transition similar to **B**. It should be noted that the 300-K remanence of **F** is almost twice as high as that for the **B**.

The low-T isothermal magnetization curves as functions of H were obtained by zero-field cooling the sample down to

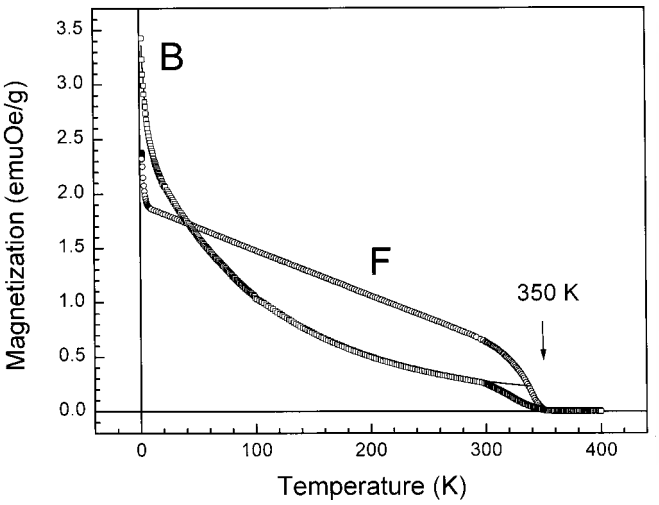

FIG. 7. Remanent magnetization as a function of T of the bulk (**B**) and film (**F**) samples. Solid line is a fit of the bulk sample experimental data (2–300 K) to sum of two exponential functions: $M(T)=0.13+1.50\times\exp(-T/4.0)+2.37\times\exp(-T/107)$.

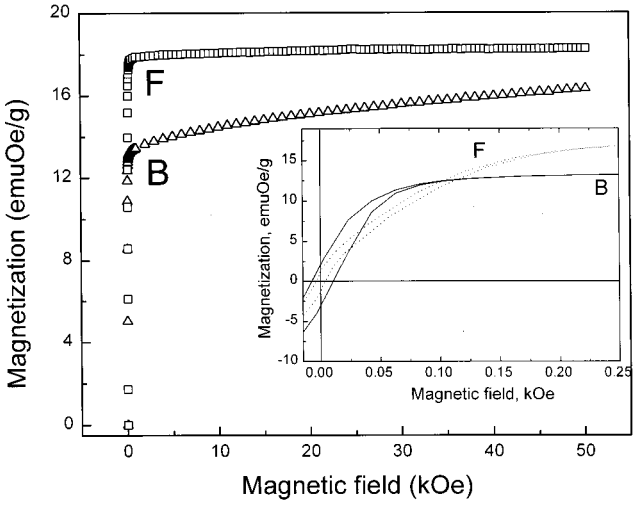

FIG. 8. Field dependence of the isothermal magnetization at 5 K of the V[TCNE]$_x$ bulk (**B**) and film (**F**) samples (the inset expands the low-field region).

5 K, and measuring the magnetization in a field up to 50 kOe. The magnetization of **B** (Fig. 8) reaches ~85% of the saturation value {16.6 emu Oe/g expected for a ferrimagnet $V[TCNE]_2\cdot 0.34(CH_2Cl_2)$ with an effective spin of $\frac{1}{2}$} in the 1000-Oe field. At higher fields the $M(H)$ gradually approaches this value; however, it does not achieve it even at 50 kOe. In contrast, **F** reaches 98% of the expected value (18.18 emu Oe/g assuming V[TCNE]$_2$ stoichiometry) at 1000 Oe (Fig. 8), demonstrating a clear tendency toward saturation at lower fields.

Hysteresis loops obtained for **B** in the ±1000-Oe field display an exponential decrease of the coercive field H_{cr} on warming (Fig. 9) from 7.8±0.1 Oe at 2 K to about 0.2 ±0.1 Oe at 300 K. Assuming that $H_{cr}(T)$ also decreases as a sum of two exponentials $H_{cr}(T)=A_1e^{-T/T_1}+A_2e^{-T/T_2}$, the

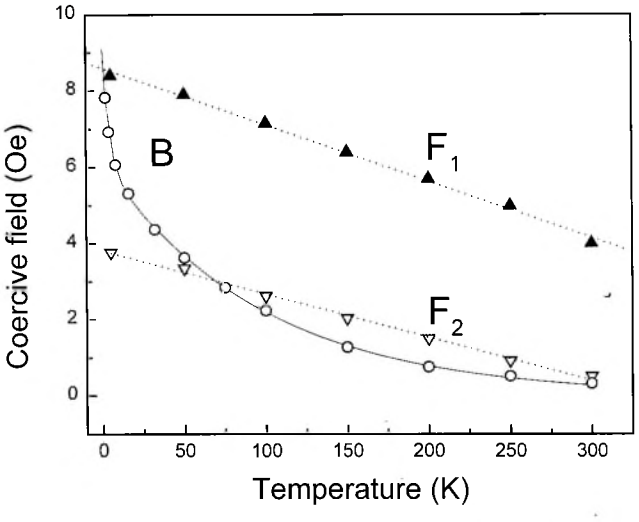

FIG. 9. Coercive field T dependence of the V[TCNE]$_x$ bulk (**B**) and film ($\mathbf{F}_1$,$\mathbf{F}_2$) samples. The sum of two exponential functions fit $M(T)=2.98\times\exp(-T/4.0)+6.13\times\exp(-T/97.3)$; dotted lines are linear fits.

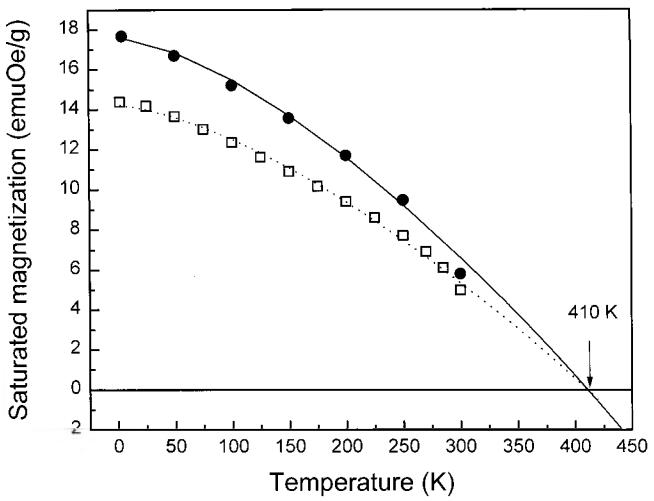

FIG. 10. Temperature dependence of saturation magnetization of $V[TCNE]_x \cdot y(CH_2Cl_2)$(**B**)(□) and $V[TCNE]_x$ film (●) samples (**F**). Solid and dotted lines represent the fits to the Bloch spin-wave theory.

best fit was obtained for $T_1=4.0$, $T_2=97$ K, and $A_1=2.98$, $A_2=6.13$ Oe. It is interesting to note that T_1 and T_2 are comparable to those determined for the remanence temperature dependence though the A_2/A_1 ratio is reduced from the $M_r(T)$ behavior.

Samples of **F** have a completely different H_{cr}. The coercive field gradually decreases with increasing temperature (Fig. 9) for two different CVD-prepared samples ($\mathbf{F}_1$ and $\mathbf{F}_2$). It should be noted that the absolute value of coercive force at low temperature may vary significantly for **F** synthesized at different conditions (different deposition rate, substrate temperature, etc.). However, their $H_{cr}(T)$ dependences as determined from fewer independent samples were found to be linear with similar slope (Fig. 9).

IV. DISCUSSION

The low-temperature saturated magnetization $M_s(T)$ is an important magnetic property. Assuming that in 1000-Oe external field the magnetization of **B** and **F** are close to their saturation values (M_s) (a better approximation for **F**), one can fit the experimental $M_s(T)$ curves (Fig. 10) to the Bloch law

$$M_s(T)=M_s(0)(1-BT^{3/2}).$$

The best fit was obtained for $B=1.2\times10^{-4}$ K$^{-3/2}$ and $M_s(0)$ values equal to 14.2 and 17.6 emu Oe/g for the **F** and **B** samples, respectively. The 17.6-emu Oe/g value is close to the 18.2 emu Oe/g expected for $V[TCNE]_2$, while for **B** it is 15% lower than the 16.6 emu Oe/g estimated for $V[TCNE]_2 \cdot 0.34(CH_2Cl_2)$.

By extrapolating $M_s(T)$ to zero the critical temperature T_c can be estimated. Interestingly, T_c is 410 K for **B** and **F**, as the best $M_s(T)$ fit was obtained with the same value of B for both samples, even though due to decomposition, the magnetization vanishes at 355 K. This value of B is 16 times higher than that for Ni (7.5×10^{-6} K$^{-3/2}$) (Ref. 9), indicating that spin waves with low wave vectors can be more easily excited in the disordered $V[TCNE]_x$ (**B** and **F**) than that in crystalline Ni. This implies that the amorphous $V[TCNE]_x$ may have a high magnon density of states at low energies.[10]

According to the spin-wave theory B is inversely proportional to $J_{ex}^{3/2}$ and, therefore, the exchange J_{ex} has similar values for both $V[TCNE]_x$ samples, which is ~100 K (assuming the simple cubic lattice[3]). Since J_{ex} depends upon the microscopic structural details like V-N distances, symmetry, and shape of the overlapping metal ion and organic radical orbitals, and the geometry of this overlapping, etc., it implies that the local V environment in the **B** and **F** forms of $V[TCNE]_x$ is very similar.

In contrast, some dc and ac magnetic properties of $V[TCNE]_x$ magnets prepared by the alternative synthetic routes are very different, suggesting that aspects of the magnetic ground state of the studied materials and/or their macroscopic (in a scale of domain and domain-walls sizes) structures are very different. For amorphous materials their difference is related to the degree of disorder introduced during the sample preparation.

An amorphous solid, especially one based on the first-row transition element, should not have any magnetic domains, due to averaging out of all sources of the anisotropy. As the domain-wall width is inversely proportional to an anisotropy constant K, the material as a whole may be considered as a domain wall when $K\rightarrow0$. However, in real amorphous systems a substantial random magnetic anisotropy may naturally arise from strain and/or composition inhomogeneities.

First-row metal-based compounds with a relatively strong exchange interaction, i.e., $J_{ex}/D_r \gg 1$ (where D_r is a random anisotropy energy), can maintain local-moment orientational correlations up to millimeters in length[10] and the aforementioned model of magnetic domains may be valid. In contrast for $J_{ex}/D_r \ll 1$ a spin-glass ground state is expected.[10]

The situation is much less clear when $J_{ex} \sim D_r$. For this case the random magnetic anisotropy (RMA) model, developed by Chudnovsky *et al.*,[11–14] predicts a formation of different magnetic phases in the material depending on the strength of an external magnetic field. This model was successfully used for interpretation of the magnetic properties of $V[TCNE]_x$ magnets synthesized using coordinating solvents, e.g., H_3CCN and C_4H_8O.[7] The character of the $M(T)$ of **B** and **F** strongly depends upon the magnitude of applied field. Therefore, the RMA model may give us an insight into microscopic parameters of $V[TCNE]_x$ magnets synthesized via different methods.

$$H=-J_{ex}\sum_{i,j} S_i\cdot S_j - D_r\sum_i (\mathbf{n}_i\cdot S_i)^2 - D_c\sum_i (S_i^z)^2 - g\mu_B\sum_i H\cdot S_i.$$

Most theoretical studies of RMA are based on the Hamiltonian H, where D_r is a random uniaxial anisotropy energy, **n** is a unit vector corresponding to a random field that points in the direction of local anisotropy, D_c is the energy of the coherent anisotropy, and J_{ex} is the exchange energy.

Assuming that $J_{ex}/D_r<1$ (weak RMA), it was shown[11] that at $T\sim 0$ the approach of the magnetization $M(H)$ toward saturation along the direction of an applied magnetic field H is equal to

$$M(H)=M_s\left(1-\frac{K^2R_H}{30A^2}\int_0^\infty dr\exp(-r/R_H)r^2C(r)\right),$$

where $C(r)$ is the correlation function of the local anisotropy directions defined by $C(r)=1$ as $r\to 0$ and $C(r)=0$ as $r\gg R_a$ (where R_a is the structural short-range order length) $R_H=[A/M_0(H+H_c)]^{1/2}$, $K=D_r/a^3$, $A=zJ/12a$, H_c is the uniaxial anisotropy field, D_r is a strength of local anisotropy, a is the mean distance between the z nearest spin sites, and M_0 is the magnitude of M.

Three different magnetic phases and $M(H)$ dependences are predicted depending on the strength of the applied external magnetic field:[11–14]

(i) for $H+H_c\gg H_{ex}$, the near collinear or quasiparamagnetic phase,

$$M(H)=M_s\left[1-\frac{1}{15}\left(\frac{H_r}{H+H_c+H_{ex}}\right)^2\right]; \quad (1)$$

(ii) for $H_s<H+H_c\ll H_{ex}$, ferromagnetic with wandering axis (FWA) phase,

$$M(H)=M_s-\frac{C}{(H+H_c)^{1/2}}; \quad (2)$$

and (iii) for $H+H_c<H_s$, the correlated spin-glass (CSG) phase, $M=0$. Here

$$H_{ex}=\frac{\alpha M_0}{R_a^2}=\frac{2zJa^2M_0}{\pi^2M_sR_a^2}, \quad (3)$$

$$C=\frac{\Lambda^2H_{ex}^{1/2}}{120\pi}\frac{\Omega}{R_a^3}, \quad (4)$$

$$\Lambda=\frac{12D_rM_s^{1/2}}{zJ}\left(\frac{R_a}{a}\right)^2. \quad (5)$$

$H_s=(H_r)^3/(H_{ex})^4$, $H_r=2n\mu_BD_rM_0/M_s^2$, and Ω is a correlation volume of anisotropy defined by

$$\Omega=\int_0^\infty 4\pi r^2C(r)dr. \quad (6)$$

Assuming that the correlation function decays exponentially, $C(r)=\exp(-r/R_a)$, one can get the apparent field dependence of magnetization[11–14]

$$M-M_s=\frac{\Lambda^2}{15p(1+p)^3},$$

where $p=[(H+H_c)/H_{ex}]^{1/2}$. For $p\to 0$ $(H\ll H_{ex})$ one has

$$M-M_s=\frac{\Lambda^2H_{ex}^{1/2}}{15(H+H_c)^{1/2}}.$$

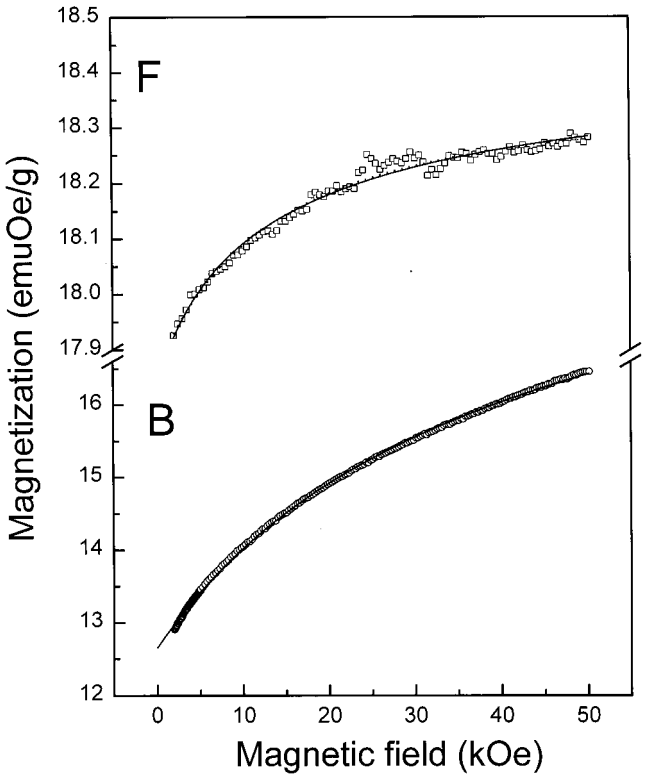

FIG. 11. Field dependence of the isothermal magnetization at 5 K of the V[TCNE]$_x$: (**B**) bulk sample, solid line, fit to the equation $M(H)=M_s-B/(H+H_c)^{1/2}$; (**F**) film sample, solid line, fit to the equation $M(H)=M_s\{1-(1/15)[H_r/(H+H_{ex}+H_c)]^2\}$; and dotted line, fit to the equation $M(H)=M_s-C/(H+H_c)^{1/2}$.

Two regimes of magnetic behavior, predicted by the RMA model, can be clearly differentiated for **B**. For $H<100$ Oe the bifurcation of FC and ZFC $M(T)$ dependences and the shift of the ac susceptibility broad maximum with frequency are characteristics of spin glass. In higher fields, **B** should exhibit properties of a FWA phase. Since T_c for **B** exceeds room temperature, H_{ex} is expected to be high, and the high-field $M(H)$ data was fit to Eq. (2), Fig. 11(a). The best agreement between experimental and calculated $M(H)$ was obtained for $M_s=21.7$ emu Oe/g, $C=1435$ emu Oe$^{3/2}$/g, and $H_c=25.4$ kOe. This agreement with RMA theory indicates that the magnetic structure in the $0.1<H<50$-kOe external field is strongly noncollinear, and **B** behaves as a ferrimagnet with a wandering axis. Its spins are tipped out of the H direction with a characteristic angle $\theta=(H_r^4/H_{ex}^3H)^{1/4}$, in which orientation may be locally preserved over length $R_\perp\ll H_{ex}R_a/2H$.

In contrast, in the fields $H<H_s-H_c$ the theory predicts that the weak RMA system should exhibit properties of a CSG. Interestingly, the critical field parameter $H_s=H_r^4/H_{ex}^3=6.43(C/M_s)^2=28.2$ kOe depends only upon two fitting parameters C and M_s. Assuming a constant anisotropy field $H_c=25.4$ kOe (the third fitting parameter), it follows that in fields less than 2.8 kOe spin-glass behavior is expected. This agrees with experimental observations and confirms that obtained RMA model parameters have reasonable values.

Prior to evaluation of the random disorder parameter

(H_r), H_{ex} should be estimated from Eq. (3). The value of zJ we take from the mean-field expression for conventional ferromagnets

$$T_c \cong (2zJ/3k)S_e(S_e+1).$$

Using $T_c = 410$ K and $S_e = \frac{1}{2}$ we obtain $zJ \sim 820$ K, yielding $J = 137$ K for $z = 6$. Assuming that $R_a/a = 25/3$,[7] $H_{ex} = 35.7$ kOe, which is within the field range studied. However, since $H_{ex} \sim (a/R_a)^2$, its value may be underestimated due to a large uncertainty in a/R_a evaluation. It may also indicate that in $H > 50$-kOe external field, the near collinear or quasiparamagnetic phase can be achieved.

From Eqs. (4) and (5), $H_s = H_r^4/H_{ex}^3 = 6.43(C/M_s)^2 = 28.2$ kOe, H_r is ~33.6 kOe and the corresponding value of $D_r \cong 2.3$ K. The coherent anisotropy energy D_c is equal to $0.33\mu_B H_c/k_B$, giving $D_c \sim 0.6$ K. Thus, $J \gg D_r \gg D_c$ in agreement with the application of the RMA model, and the obtained anisotropy and exchange parameters have consistent values. A large value of the random anisotropy energy D_r is also consistent with a substantial degree of disorder in this system originating from solvent molecules incorporated in its structure. On the other hand, D_r for $V[TCNE]_x \cdot y(CH_2Cl_2)$ is considerably lower than the values of 5.5 K for both $V[TCNE]_x \cdot y(THF)$ or $V[TCNE]_x \cdot y(H_3CCN)$.[7]

The higher than expected value of M_s may derive from a higher than $\frac{1}{2}$ average effective spin {assuming that defects modulate a charge transfer from V^{II} to $[TCNE]^{\cdot -}$ (as proposed above)} or from nonstoichiometry.

From Fig. 8, the field dependence of magnetization approaching saturation $M(H)$ for **F** is very different from that for **B**. The experimental data can almost equally well be fitted by both Eqs. (1) and (2) [Fig. 11(b)]. The best fit for Eq. (2) was obtained with $M_s = 18.5$ emu Oe/g, $C = 53.8$ emu $Oe^{3/2}$/g, and $H_c = 6.3$ kOe. Both parameters H_c and C (which are proportional to H_r^2) are substantially lower than those for **B** with respect to **F**. Preliminary electron-spin-resonance studies of **F** show an intensive signal near $g = 2$. Lack of other signals with $g \neq 2$ can indicate that the coherent magnetic anisotropy is very small, and therefore, a large difference between H_c in the film and bulk samples is not expected. The analyses of $V[TCNE]_x$ magnets prepared using coordinating H_3CCN and THF solvents in the framework of RMA also gave H_c close to that for the bulk sample.[7] Thus, the parameters obtained by fitting to Eq. (2) do not completely reflect the real situation in **B**.

The best fit to Eq. (1) for **F** at 5 K was obtained with $M_s = 18.3$ emu Oe/g, $H_r = 16.5$ kOe, and $H_c + H_{ex} = 26.6$ kOe. M_s is very close to the value that one should expect for the effective spin of $\frac{1}{2}$. It is consistent with the lack of defects originating from the solvent substitution and/or blocking of the coordination sites. The parameter $H_c + H_{ex}$ is only 1.2 kOe higher than H_c for **B**. As it was mentioned above, H_c is expected to be similar in value to those obtained for $V[TCNE]_x$ prepared in different ways. Therefore, it is conceivable to assume that in the film, the H_{ex} parameter should be much smaller than that for the bulk. Since T_c is the same for **B** and **F**, the a/R_a ratio in the film is smaller, and the correlation length R_a is higher. Interestingly, another parameter of the RMA model H_r is half that of **F** with respect to **B**, which is also consistent with less disorder in **F** and higher value of R_a. The small value of H_{ex} is also supported by the fact that in $H > 5$ kOe, $M(H)$ for **F** can be fitted to Eq. (1), which is valid only for $H \gg H_{ex}$.

Accordingly to Chudnovsky *et al.*,[12,16] a weak coherent anisotropy, satisfying $\lambda_c^{1/2} > \lambda_r^2$ [where $\lambda_c = (2/15)^{1/2}(H_c/H_{ex})$, $\lambda_r = (2/15)^{1/2}(H_r/H_{ex})$] destroys the correlated spin-glass state (CSG). Assuming $H_{ex} = 6$ and $H_c = 20.6$ kOe, $\lambda_c^{1/2}$ is only slightly higher than λ_r^2. Taking into account that our estimation of H_{ex} is very rough, the possibility of the CSG in the film sample in $H = 0$ cannot be completely ruled out. However, the character of the dc irreversibility as well as the lack of ac susceptibility frequency dependence suggests that the nature of this phase in **F** may be different from that for **B**.

Evidently, application of a relatively weak external field may destroy the CSG state and **F** becomes a FWA. Since H_{ex} in **F** is apparently much smaller than in **B**, and the FWA phase is limited by the condition $H + H_c \ll H_{ex}$ this phase survives only in a relatively narrow field interval. On further field increase, the FWA transforms into the nearly collinear ferromagnet (in our case, ferrimagnet) phase.

Interestingly, the temperature dependences of remanence and coercive field are very different in the film and bulk samples, again suggesting that these materials may have different ground states in low magnetic fields. We speculate that the solution—prepared bulk samples (**B**)—most probably consists of randomly oriented atomic clusters. The large irreversibility in the dc magnetization of **F** may be explained by magnetic domain freezing instead of a spin-glass state.[15] However, to prove these assumptions, additional structural and magnetostructural information is of great importance.

V. CONCLUSIONS

We have reported $M(H,T)$ for two members of the $V[TCNE]_x$ family magnets, namely, prepared using the noncoordinating CH_2Cl_2 solvent and prepared via solvent-free CVD. Since the irreversible magnetostructural transition occurs almost at the same temperature for both materials, and the extrapolated values of T_c obtained from $M_s(T)$ dependences coincide for both substances, the presence of noncoordinating solvents (like CH_2Cl_2) does not substantially influence T_c. However, the noncoordinating solvent creates additional structural disorder resulting in a spin-glass behavior at liquid-helium temperatures in low magnetic fields ($H < 100$ Oe), small remanence, and vanishing H_{cr} at room temperature. Hence, the properties of $V[TCNE]_x \cdot y(CH_2Cl_2)$ are very similar to those of the other members of this family of magnets produced using C_4H_8O and H_3CCN.[7]

In contrast, as the CVD film lacks these structural defects and has increased structural order, this leads to a totally different $M(H)$ dependence approaching saturation as well as different behavior of $\chi''(T)$, $H_{cr}(T)$, and $M_r(T)$. The de-

gree of disorder of both studied compounds was analyzed in the framework of the random magnetic anisotropy model, which provided a quantitative confirmation of this assumption.

Thus, the reliable technique of $V[TCNE]_x$ film deposition with reproducible magnetic properties and enhanced stability was proposed, which makes this material potentially applicable for device fabrication.

ACKNOWLEDGMENTS

The authors gratefully acknowledge the continued support of DOE DMS Grant Nos. DE FG 02-86BR45271 and DE FG 03-93ER45504. The NSF Grant No. CHE-9002690 and the University of Utah Institutional Funds Committee are acknowledged for providing partial support for high-resolution mass spectroscopy equipment.

[1] V. I. Ovcharenko and R. Z. Sagdev, Russ. Chem. Rev. **68**, 345 (1999); J. S. Miller and A. J. Epstein, Chem. Commun. (Cambridge) **1998**, 1319; W. Plass, Chem. Unserer Zeit **32**, 323 (1998); P. Day, J. Chem. Soc. Dalton Trans. **1997**, 701; J. S. Miller and A. J. Epstein, Chem. Eng. News **73**, 30 (1995); Adv. Chem. Ser. **245**, 161 (1995); Angew. Chem. Int. Ed. Engl. **33**, 385 (1994); M. Kinoshita, Jpn. J. Appl. Phys., Part 1 **33**, 5718 (1994); D. Gatteschi, Adv. Mater. **6**, 635 (1994); O. Kahn, *Molecular Magnetism* (VCH, New York, 1993).

[2] Room-temperature molecule-based magnets with spins only residing on metal ions have also been reported. S. Ferlay, T. Mallah, R. Ouahes, P. Veillet, and M. Verdaguer, Nature (London) **378**, 701 (1995); Ø. Hatlevik, W. E. Buschmann, J. Zhang, J. L. Manson, and J. S. Miller, Adv. Mater. **11**, 914 (1999); S. D. Holmes and G. Girolami, J. Am. Chem. Soc. **121**, 5593 (1999).

[3] J. M. Manriquez, G. T. Yee, R. S. McLean, A. J. Epstein, and J. S. Miller, Science **252**, 1415 (1991); J. S. Miller, G. T. Yee, J. M. Manriquez, and A. J. Epstein, in *Proceedings of Nobel Symposium Number NS-81, Conjugated Polymers and Related Materials: The Interconnection of Chemical and Electronic Structure*, edited by W. R. Salaneck, I. Lundsrom, and B. Rånby (Oxford University, New York, 1993), p. 461.

[4] J. Zhang, P. Zhou, W. B. Brinckerhoff, A. J. Epstein, C. Vazquez, R. S. McLean, and J. S. Miller, ACS Symp. Ser. **644**, 311 (1996).

[5] K. I. Pokhodnya, A. J. Epstein, and J. S. Miller, Adv. Mater. **12**, 410 (2000); D. de Caro, M. Basso-Bert, J. Sakah, H. Casellas, J.-P. Legros, L. Valade, and P. Cassoux, Chem. Mater. **12**, 587 (2000).

[6] J. S. Miller and A. J. Epstein, Mol. Cryst. Liq. Cryst. Sci. Technol., Sect. A **233**, 171 (1993).

[7] P. Zhou, B. G. Morin, J. S. Miller, and A. J. Epstein, Phys. Rev. B **48**, 1325 (1993); P. Zhou, S. M. Long, J. S. Miller, and A. J. Epstein, Phys. Lett. A **181**, 71 (1993).

[8] According to our measurements the following masses appear in the mass spectrum of TCNE: 26, 38, 48, 50, 62, 64, 76, 77, 102, 114, and 128.

[9] Chin-Wen Chen, *Magnetism and Metallurgy of Soft Magnetic Materials* (Dover, New York, 1977), p. 51.

[10] T. Kaneyoshi, *Introduction to Amorphous Magnets* (World Scientific Singapore, 1992), p. 107.

[11] E. M. Chudnovsky, W. M. Saslow, and R. A. Serota, Phys. Rev. B **33**, 251 (1986).

[12] E. M. Chudnovsky and R. A. Serota, Phys. Rev. B **26**, 2697 (1982); J. Phys. C **16**, 4181 (1983).

[13] E. M. Chudnovsky, Phys. Rev. B **33**, 2021 (1986).

[14] E. M. Chudnovsky, J. Magn. Magn. Mater. **79**, 127 (1989).

[15] X. L. Wang, J. Horvat, H. K. Liu, and S. X. Dou, Solid State Commun. **108**, 661 (1998).

[16] J. Tejada, B. Martinez, A. Labarta, and E. M. Chudnovsky, Phys. Rev. B **44**, 7698 (1991).